ELSEVIER

Quaternary Science Reviews 23 (2004) 481–498

QSR

Investigation of the spatio-temporal variability in Eurasian Late Quaternary loess–paleosol sequences using a coupled atmosphere–ocean general circulation model

Andrew B.G. Bush[a,*], Edward C. Little[b], Dean Rokosh[c], Dustin White[d], Nathanial W. Rutter[a]

[a] *Department of Earth and Atmospheric Sciences, 126 Earth Sciences Building, University of Alberta, Edmonton, Alberta, Canada T6G 2E3*
[b] *Canada–Nunavut Geoscience Office, Box 2319, Iqaluit, Nunavut, Canada X0A 0H0*
[c] *Department of Physics, P-412 Avadh Bhatia Physics Lab, University of Alberta, Edmonton, Alberta, Canada T6G 2J1*
[d] *Department of Anthropology, 13-15 HM Tory Building, University of Alberta, Edmonton, Alberta, Canada T6G 2H4*

Received 3 June 2003; accepted 12 August 2003

Abstract

Loess–paleosol sequences from across the Asian interior indicate that Late Quaternary glacial periods were primarily characterized by loess deposition, although in some regions weakly developed paleosols also developed. During interglacial periods, paleosol formation dominated in most, but not all, areas. Possible reasons for this complex spatio-temporal variability of loess–paleosol deposition are investigated through the use of a coupled atmosphere–ocean general circulation model configured for the Last Glacial Maximum (LGM) and for the early–mid-Holocene.

Downstream modification of the westerly trade winds by the Fennoscandian ice sheet affected climate means across much of the Asian interior. In particular, weaker horizontal winds, enhanced atmospheric subsidence, and significantly reduced moisture transport combined to dry the continental interior to such a degree that there was a northeastward expansion of the cool, semi-arid, B-climate zone of the Köppen classification. Orographic precipitation triggered by the Fennoscandian ice sheet, however, increased precipitation and snow melt amounts in the proximity of the ice sheet margin. Glacial climate over the Chinese Loess Plateau, on the other hand, was less susceptible to downstream effects and was determined primarily by changes in the south Asian monsoon. During the more seasonal early Holocene, there were latitude-dependent changes in soil moisture, with significant wetting across low-mid-latitudes and drying in the mid-high latitudes of the Siberian Plain. Our simulated spatio-temporal variability of the hydrological cycle may, therefore, give insight into the interpretation of the complex sediment records from the Asian interior that serve as proxies for paleoclimatic reconstructions.

1. Introduction

Terrestrial records from the Chinese Loess Plateau (~36–37°N, ~107–110°E; Fig. 1) have yielded a wealth of proxy data from which it is possible to reconstruct climatic conditions through the Quaternary (e.g., Rutter, 1992; Vandenberghe et al., 1997; Sun et al., 1999; Lu et al., 1999, 2000). Alternating beds of loess and paleosols provide a direct terrestrial fingerprint of glacial and interglacial climates and because they correlate, in general, with oxygen isotope records from deep sea cores (e.g., Porter and An, 1995; Guo et al., 1998; Rack et al., 2000) they have been used as a proxy for global climate.

During the Holocene, it has been suggested that climate is one of the key factors that governed soil formation on the Loess Plateau (Maher et al., 2003). The geographic location of the Plateau, however, places it within the sphere of influence of the summer and winter South Asian monsoons (e.g., Tarasov et al., 2000a). Changes in monsoon winds and precipitation through a glacial cycle have likely played some role in the formation of these loess/paleosol sequences (e.g., An et al., 2000; Tarasov et al., 2000a; Bush et al., 2002).

Terrestrial records from across the Asian interior, remote from the direct influence of the monsoon,

*Corresponding author. Tel.: +1-780-492-3265; fax: +1-780-492-2030.
E-mail address: andrew.bush@ualberta.ca (A.B.G. Bush).

0277-3791/$ - see front matter © 2003 Elsevier Ltd. All rights reserved.
doi:10.1016/j.quascirev.2003.08.009

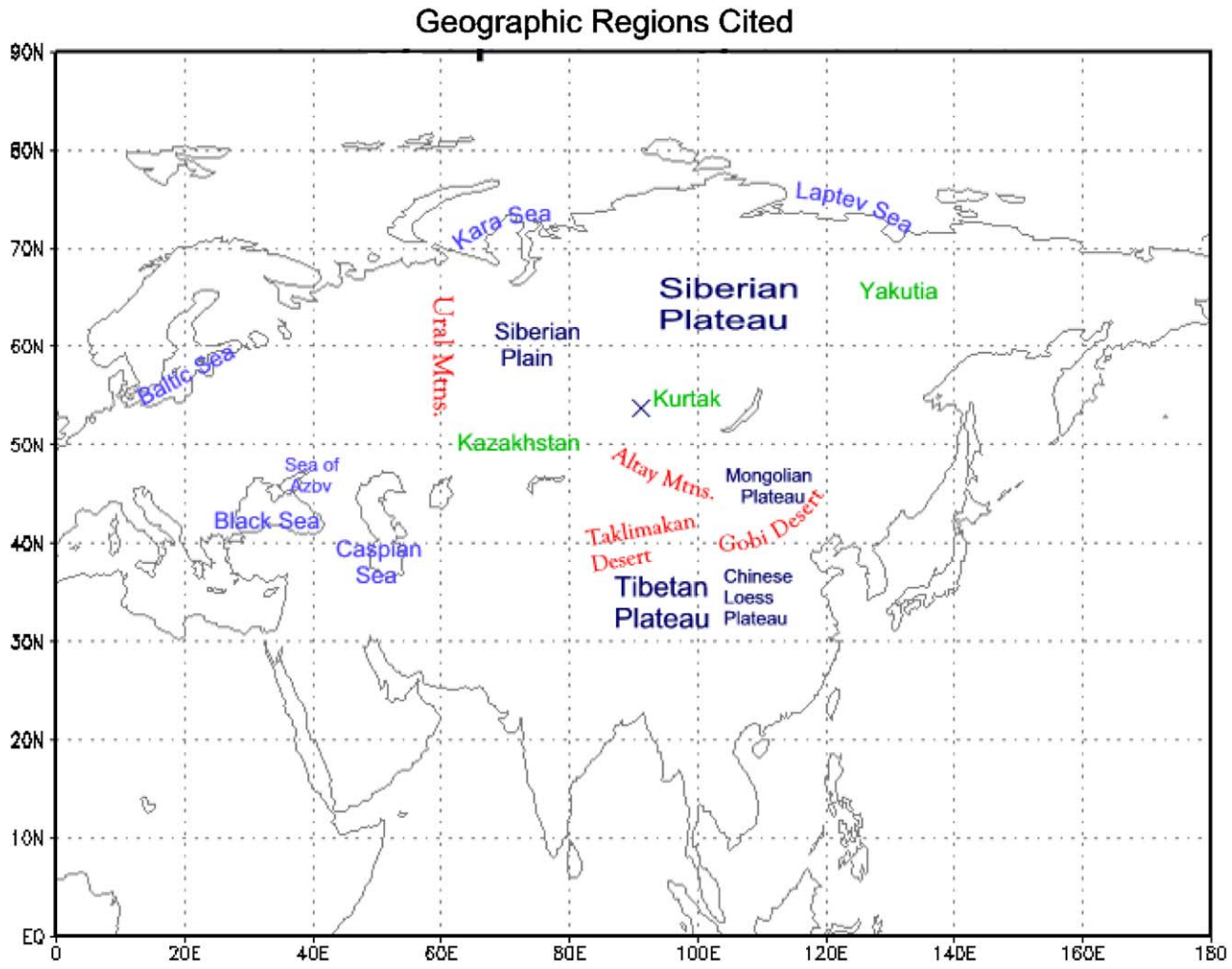

Fig. 1. A schematic map of the geographic sites referenced throughout the text. Plateaus are indicated in dark blue, seas in light blue, deserts and mountains in red, and regions and cities (i.e., Kurtak) in green. The latitudes and longitudes of some regions are given in the text but the reader is encouraged to refer to this figure for georeferencing.

indicate that climatic change during the last glacial–interglacial cycle was similar across the continent despite the fact that the data were gathered from quite different geographic settings (Rutter et al., 2003). Although the proxy records from the Asian interior correlate quite well with those from the Loess Plateau, there are some interesting regional differences. For example, during glacial periods loess beds dominate across Asia and on the Loess Plateau, although weakly developed paleosols are also seen in central Siberia and the Loess Plateau (Rutter et al., 2003). During the interglacial period of oxygen isotope stage 5, for example, records from both Kurtak in central Siberia (55°06′N, 91°24′E) and the Loess Plateau show that paleosol formation dominates over loess deposition (Rutter et al., 2003). Furthermore, Holocene data from the Loess Plateau indicate that even within an interglacial, there is a transition from moist early Holocene conditions to arid, mid-Holocene conditions (e.g., Tarasov et al., 2000a; Liu et al., 2002; Chen et al., 2003). This complex spatio-temporal pattern of loess–paleosol accumulation, illustrated in Fig. 2, is likely related to regional climate changes that are highly dependent on insolation, atmospheric composition, and changes in atmospheric circulation patterns (e.g., Kohfeld and Harrison, 2000; Lu and Sun, 2000; Xiao et al., 2002). If true, what are the factors responsible for these changes across the Asian interior through a glacial cycle?

Two factors that impact global temperature and precipitation are the greenhouse gas loading of the atmosphere and insolation changes through time. Reduction of atmospheric carbon dioxide and water vapour during glacial periods reduces global atmospheric and oceanic temperatures as well as global precipitation and evaporation. These changes would increase dust loading of the atmosphere (e.g., Thompson et al., 1995) and encourage the expansion of desert regions (e.g., Sun et al., 1995, 1998; Rokosh et al., 2003). However, such changes would be global in extent and, although differences in the magnitude of regional

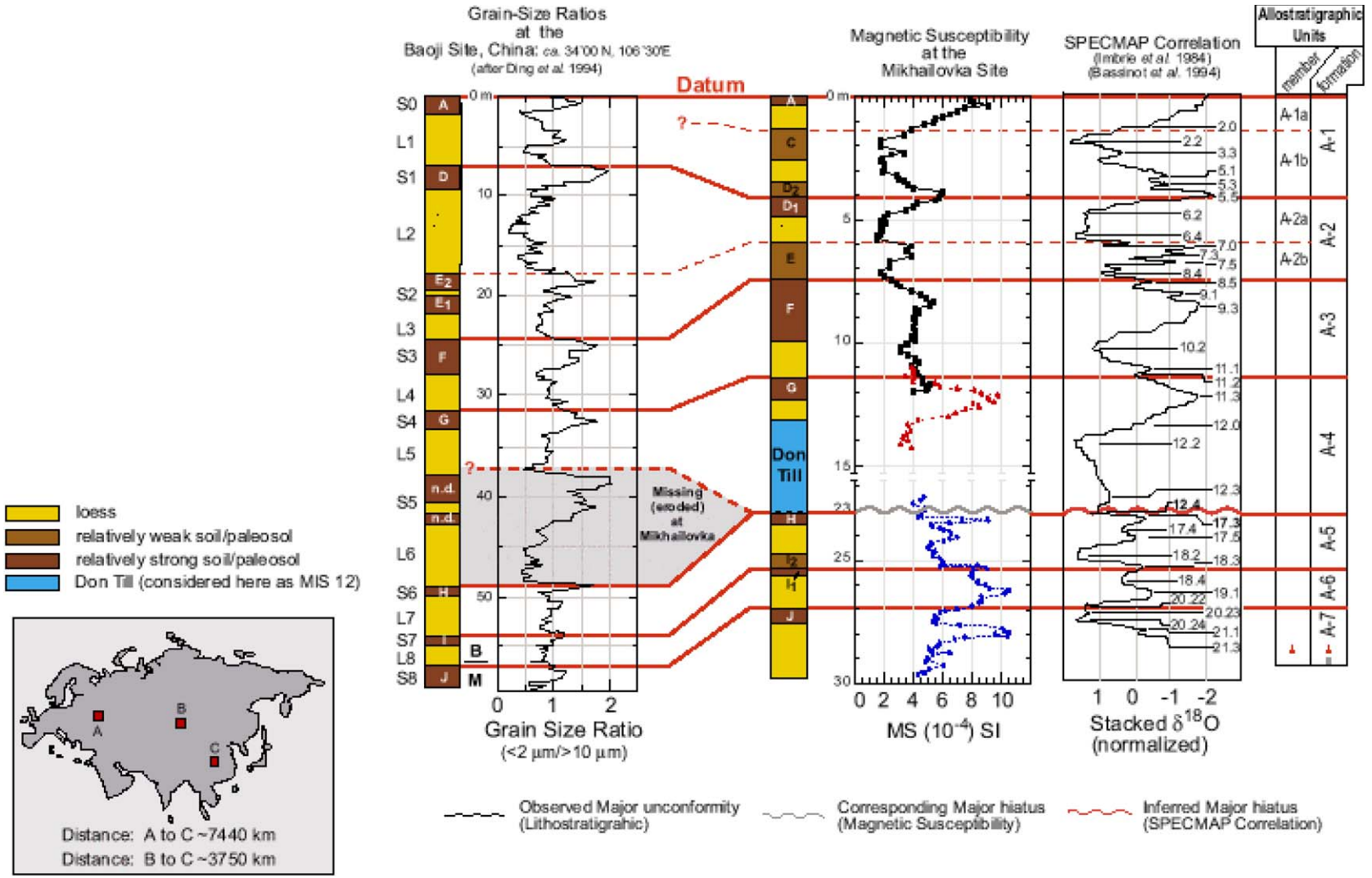

Fig. 2. Allostratigraphic scheme applied to the stratigraphy and magnetic susceptibility of a record from Mikhailova (50°06′N; 43°14′E), and the orbitally tuned grain-size ratio record at Baoji, China (Ding et al., 1994). For the Baoji striplog, both Chinese paleosol–loess designators and Russian Plain paleosol designators are used for comparison. Allostratigraphic correlations are based on the comparison of both pedostratigraphic position and grain-size/magnetic susceptibility trend similarities at Baoji and Mikhailovka, respectively.

responses may occur, the sign of the climate anomaly would, in general, be the same throughout a continental interior. Insolation changes also affect atmospheric temperature and hence the hydrological cycle, but they are independent of longitude and are, during the late Quaternary, relatively uniform in the latitudinal belt of interest ($\sim 40^\circ$N–50°N). Therefore, differences between records from the central Asian interior and from the Loess Plateau most likely arise from differences in atmospheric circulation.

In today's climate, topography plays a critical role in maintaining regional climate zones. For example, orographic precipitation on the windward side of mountains and dry adiabatic descent on the lee side of mountains maintains distinctly different climate regimes on either side of steep topography. Very high and expansive topography, such as the Tibetan Plateau, affects climatological winds on a hemispheric scale through the generation of stationary planetary long-waves. In general, these waves are generated from latitudinal perturbations of westerly winds by the presence of topography or by oceanic-to-continental pressure contrasts. Since the magnitude of the Coriolis parameter varies with latitude, and since the sum of the Coriolis parameter and the flow's relative vorticity is a conserved quantity (e.g., Holton, 1979), such perturbations generate curvature and oscillations in the flow on a hemispheric scale. In fact, the presence of the Tibetan Plateau has been shown to be the primary cause of aridity over the Asian Steppe east of the Caspian Sea through its generation of such a long planetary wave and its associated large-scale subsidence over the Asian interior (Broccoli and Manabe, 1992). The south Asian monsoon is also fundamentally influenced by the presence of the Tibetan Plateau (e.g., Hahn and Manabe, 1975; Kutzbach et al., 1989; Broccoli and Manabe, 1992). During the summer months, the enormous amount of latent heat released above the Plateau triggers westward propagating Rossby waves in the atmosphere whose associated pattern of subsidence is responsible for maintaining arid conditions to the west of the monsoon region (Hoskins and Rodwell, 1995; Rodwell and Hoskins, 1995). In addition, the generation of planetary waves by topography, combined with the temporal variation of incoming solar radiation, causes the latitudes of the westerly jets to fluctuate from month to month and from year to year (Limpasuvan and Hartmann, 2000). An interannual manifestation of such fluctuations in the Northern Hemisphere is the North Atlantic/Arctic oscillation (e.g., Thompson and Wallace, 2000).

Topography is therefore a key element in hemispheric climate variability as well as in the maintenance of modern regional climate. During glacial periods, the presence of massive continental ice sheets that can be kilometers thick and thousands of kilometers in extent dramatically alters topography. Modification of atmospheric flow patterns by the presence of such ice sheets has been investigated previously (e.g., Hahn and Manabe, 1975; Crowley, 1984; Wright et al., 1993; Hall et al., 1996; Bush and Philander, 1999). What is less well known is the extent to which such ice sheets affect climate across the Asian interior, and whether or not the existing terrestrial climate proxy records reflect a degree of spatial variability (or coherence) that may be linked to regional changes in atmospheric circulation.

We investigate this question by examining the climate at the LGM ($\sim 21,000$ years BP), at 9000 years BP, and at 6000 years BP as simulated by a coupled atmosphere–ocean general circulation model. Comparison to a modern control simulation reveals climate anomalies at these times. Note that all dates for the simulations are in calendar years before present. When it is necessary to invoke radiocarbon years for data intercomparison, calendar years will also be given in order to put the simulation results in context. In Section 2, we describe the models used and the configuration of them in the simulations. In Section 3, we present comparative results that are discussed in Section 4. Concluding remarks are made in Section 5.

2. The models and their configuration

All simulations were performed by an atmospheric general circulation model (GCM; Gordon and Stern, 1982) that is coupled both dynamically and thermodynamically to an ocean general circulation model (Pacanowski et al., 1991). The atmospheric model has 14 unevenly spaced levels in the vertical, with the lowest model level approximately 30 meters above the surface in a standard atmosphere. The equivalent spatial resolution is 3.75° in longitude by 2.25° in latitude (at the equator). The ocean model has comparable resolution at 3.62° in longitude and 2° in latitude with 15 unevenly spaced vertical levels, more than half of which are in the upper kilometer of the ocean in order to better simulate thermocline dynamics. The models interact each day in a staggered integration scheme in which boundary condition variables (averaged over the day) are passed between the models. Variables passed from the ocean model to the atmospheric model are sea surface temperature (SST) and surface current velocities. Variables passed from the atmospheric model to the ocean model are net radiation, net sensible and latent heat fluxes, net freshwater flux, and wind stress. A thermodynamic formulation of sea ice (Fanning and Weaver, 1996) that includes brine rejection, is incorporated using the same grid as the ocean model. The initial condition of the oceans is the modern climatological mean temperature and salinity fields (Levitus, 1982) and is the same in each simulation. Orbital parameters are

specified for 6000 BP (mid-Holocene), 9000 BP (early Holocene), and 21,000 BP (LGM) according to Berger and Loutre (1991).

Land surface albedos are specified as modern in all simulations except for the LGM, in which values were prescribed from CLIMAP (1981). Sensitivity experiments by the Palaeoclimate Modelling Intercomparison Project (PMIP) indicate that model results over Europe, at least, are relatively insensitive to the vegetation cover (Masson et al., 1999). In comparison, the early-mid-Holocene simulations by the COHMAP group (e.g., Wright et al., 1993) linearly interpolated land surface albedo values between modern and LGM values. There will obviously be some degree of error in paleo-albedo reconstructions, but the reader should keep in mind that any changes in the early and middle Holocene simulations may not be ascribed to any change in the land surface albedo.

Glacier extent and elevation in the LGM and 9000 BP simulations are derived from Peltier (1994), and land surface albedo values for the ice sheets are prescribed to be 0.6. Greenhouse gas concentration in the control and Holocene simulations was set at preindustrial levels (300 ppm) and reduced to 200 ppm in the LGM simulation. Continental margins in the LGM simulation reflect a 120 m drop in sea level (Fairbanks, 1989).

Diffusivities in the ocean model are decreased in order to preserve a realistic tropical climatology (e.g., Meehl et al., 2001) and a turbulent mixing scheme based on the local Richardson number is used (Pacanowsi and Philander, 1981). All integrations are 70 years in length so that changes in surface ocean characteristics are well simulated, and, in the experiments, show changes that are dynamically consistent with the altered boundary condition forcing. We therefore do not address the issue of any changes in benthic ocean currents, although changes in deep water formation are captured since convection is a surface-driven process. Feedbacks of any change in benthic currents on the surface ocean are therefore not captured. However, ocean models are not at present equipped with parameterizations that correctly capture the timescales and dynamics of diapycnal mixing now observed in the rather energetic abyssal ocean (e.g., Munk and Wunsch, 1998; Wunsch, 2000; see a review in Toole and McDougall, 2001). We therefore focus on the atmosphere and upper ocean dynamics for the purposes of this study.

3. Results

The 2-cm annual mean soil moisture contour is used in this study as a proxy for desert margins. Soil moisture is used because all the variables that determine the hydrological cycle at each grid point at every time step are incorporated in its computation. In particular, a prognostic equation for soil moisture is computed every 216 seconds according to the sum of precipitation and snowmelt minus evaporation. The temperature dependence of each of these quantities is therefore intrinsic to the calculation through sensible and latent heat fluxes. In addition, soil moisture feedback on regional precipitation plays an important role across Asia. For further technical details of the scheme see, e.g., Washington and Parkinson (1986).

The choice of the 2-cm soil moisture level as a desert margin is arbitrary but delivers desert margins in the control simulation that are closest to reality. As discussed in Broccoli and Manabe (1992), there is a close correlation of the Köppen climate classification with simulated soil moisture values, particularly in regions exhibiting category B (cool and semi-arid) climates. In comparison to climate data, the control simulation reasonably reproduces today's climate zones as defined by the Köppen scheme (Fig. 3).

The proxy desert margin in the control simulation encompasses much of the Taklimakan (~38–40°N, 76–90°E) and Gobi (~40–47°N, 100–118°E) deserts north and west of the Loess Plateau (Fig. 4a; see also Bush et al., 2002). Changes in the position of this contour are therefore interpreted as movement of the desert margin.

In the mid-Holocene (Fig. 4b), statistically significant wetting of the southeast desert margin has been demonstrated previously (Bush et al., 2002). In the early Holocene, substantial wetting of the soil shrinks the desert margin significantly (Fig. 4c). Temperature and precipitation changes in the region are sufficient to switch the Köppen climate classification of this area from a BWk climate (dry/arid and cool) in the control simulation to a Dwc climate (subarctic with dry winters but significant summer precipitation) at 9000 years BP. In contrast, significant drying and desert margin expansion occurs in the LGM simulation (Fig. 4d; note that the drying of this region is more enhanced than in the shorter simulation analyzed in Bush et al. (2002) although the overall spatial pattern of continental drying is similar).

Simulated wetting/drying has a latitudinal dependence. Low latitude regions (~35° to −45°N) in the early mid Holocene simulations are primarily wetter, whereas north central Asian regions (~50° to −70°N, 60° to −110°E) are drier. In the LGM simulation, most of central Asia from 35–65°N is drier than modern day values but the region bordering the Fennoscandian ice sheet is wetter. A *t*-test for statistical significance (Press et al., 1992) of these spatial patterns of wetting/drying indicates that most of the changes are significant at greater than the 99% level (Fig. 5). Regions where the simulated changes produce low values on the *t*-test are north of the Caspian Sea, where there is little or no simulated change in mean soil moisture (cf. Fig. 4) and

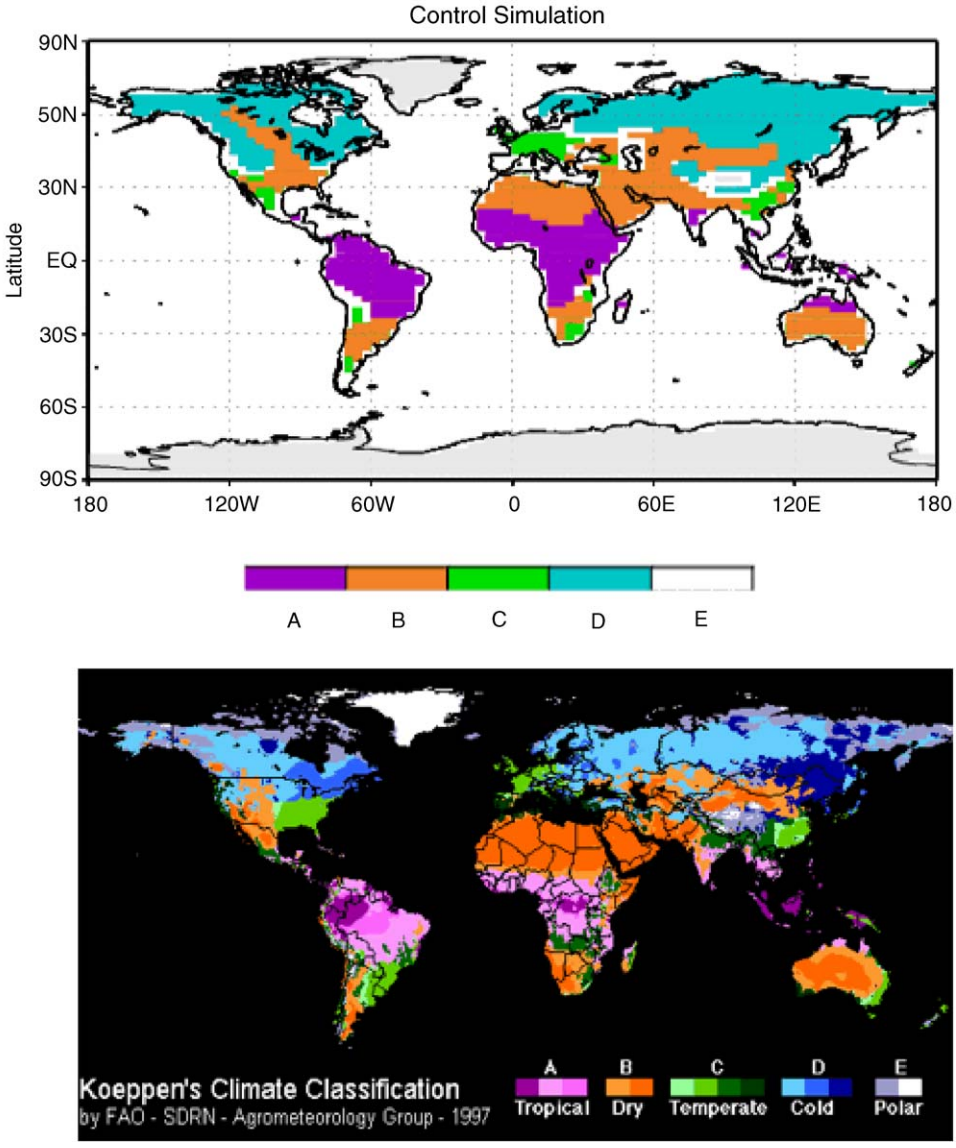

Fig. 3. A comparison of the Köppen climate classification simulated by the model (top panel) and from observations (lower panel). Subclassifications within each climate zone are not included in the simulated data. Glaciated regions appear in grey, and the Highland classification is in white. Those data points that failed to classify in any of the categories also appear in white.

hence small or zero values are computed in the *t*-test. For most of central Asia, however, the simulated changes are more than 99% statistically significant, particularly in the LGM simulation. An equivalent analysis of precipitation yields comparable levels of confidence across the entire Asian interior in the 9000 BP and LGM simulations. The simulations therefore produce statistically significant, spatio-temporal variability in the soil moisture field.

Although the Asian interior is remote from the Atlantic Ocean, the trade westerlies transport a sufficient amount of water such that most of the continental interior is not dry today. It is the presence of significantly large mountain ranges that shape and position the arid regions (Fig. 6a). The Tibetan Plateau splits the annual mean, westerly water vapour transport into northern and southern branches, and it is this splitting that positions the arid zone of central Asia north of the Himalaya (Broccoli and Manabe, 1992). Water vapour transport significantly increased over southeastern Asia at 9000 BP because of enhanced summer monsoon winds (Fig. 6b). At the LGM, water vapour transport was decreased across all of the Asian interior because of orographic blocking of the trade westerlies by the Fennoscandian ice sheet (Fig. 6c). Significant contraction and expansion of the Taklimakan and Gobi deserts in the 9000 BP and LGM simulations, respectively, are evident from the 2-cm soil moisture contour map (cf. Fig. 4) and is in good agreement with estimates of Late Quaternary desert

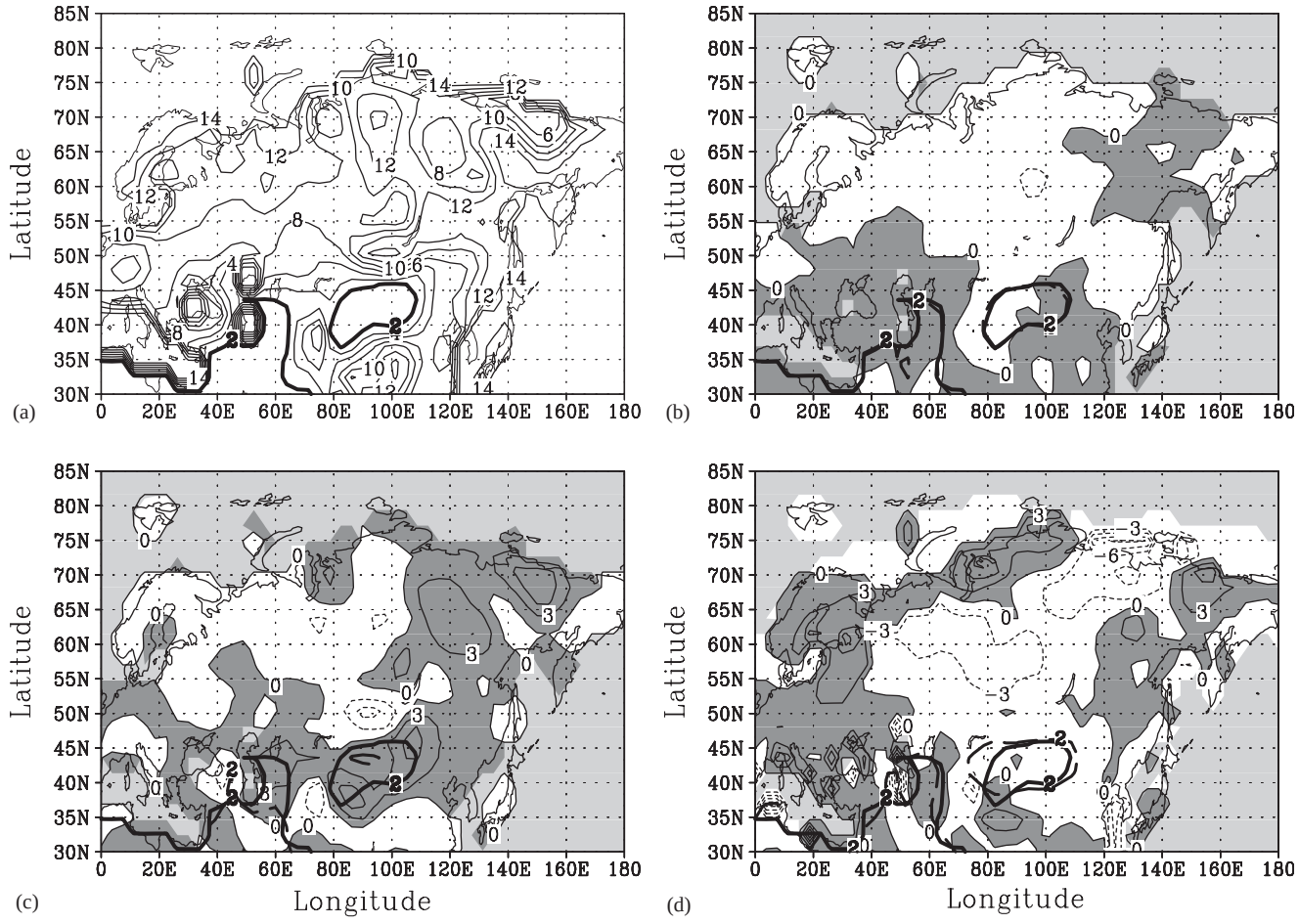

Fig. 4. (a) Simulated annual mean soil moisture for today, with the 2-cm contour in solid bold (shown in all panels for reference). Difference plots (experiment minus control) are shown for (b) the mid-Holocene, (c) the early Holocene, and (d) the Last Glacial Maximum. Units are centimeters of water. The contour intervals are 2 cm in (a) and 3 cm in (b)–(d). Dark shading in (b)–(d) indicates regions that were wetter than today, whereas white regions were drier. The 2-cm contour from the control simulation is shown in all panels by a solid bold contour. The 2-cm contour from each experiment is shown by a dashed bold contour.

margin migration (e.g., Sun et al., 1998; Bush et al., 2002; Rokosh et al., 2003).

Focusing on north-central Asia between 45–65°N and 60°–120°E, there is an increase in summer precipitation in the early and mid-Holocene simulations, although there is also increased summer evaporation from warmer seasonal temperatures (Figs. 7a–c). The reduction in soil moisture across much of the West Siberian Plain (between the Ural mountains and the Siberian Plateau, north of 50°N; cf. Fig. 4) arises from the reduction in winter–spring precipitation in all three experiments. In the LGM simulation, reduced winter–spring rainfall in this region is a consequence of both globally reduced precipitation and reduced moisture transport into the region due to upstream blocking by the Fennoscandian ice sheet. In the early and mid-Holocene simulations, reduced winter–spring rainfall (most evident from January to April) is a consequence of colder winters and a reduced saturation vapour pressure. Despite an increase in winter snowfall in all three experiments (Fig. 7c), the equivalent amount of additional water does not compensate for the reduced rainfall in an annual mean. Seasonal temperatures therefore play an important role in regulating the soil moisture across northern Asia.

Farther south, between 35°N and 45°N, the results are a little different (Figs. 7d–f). At these latitudes, which are typically characterized by semi-arid, type B climates (with some wetter type D climates close to high topography) there is very little winter precipitation so changes between November and March are minimal. In the summertime, however, increased precipitation in the early and mid-Holocene simulations increases the soil moisture, particularly in the 9000 BP simulation where there is a 49% increase (averaged between 60–120°E; cf. Figs. 4b,c). Reduction of year-round precipitation in the LGM simulation dominates the hydrologic budget so the area-averaged soil moisture is 15% less than today.

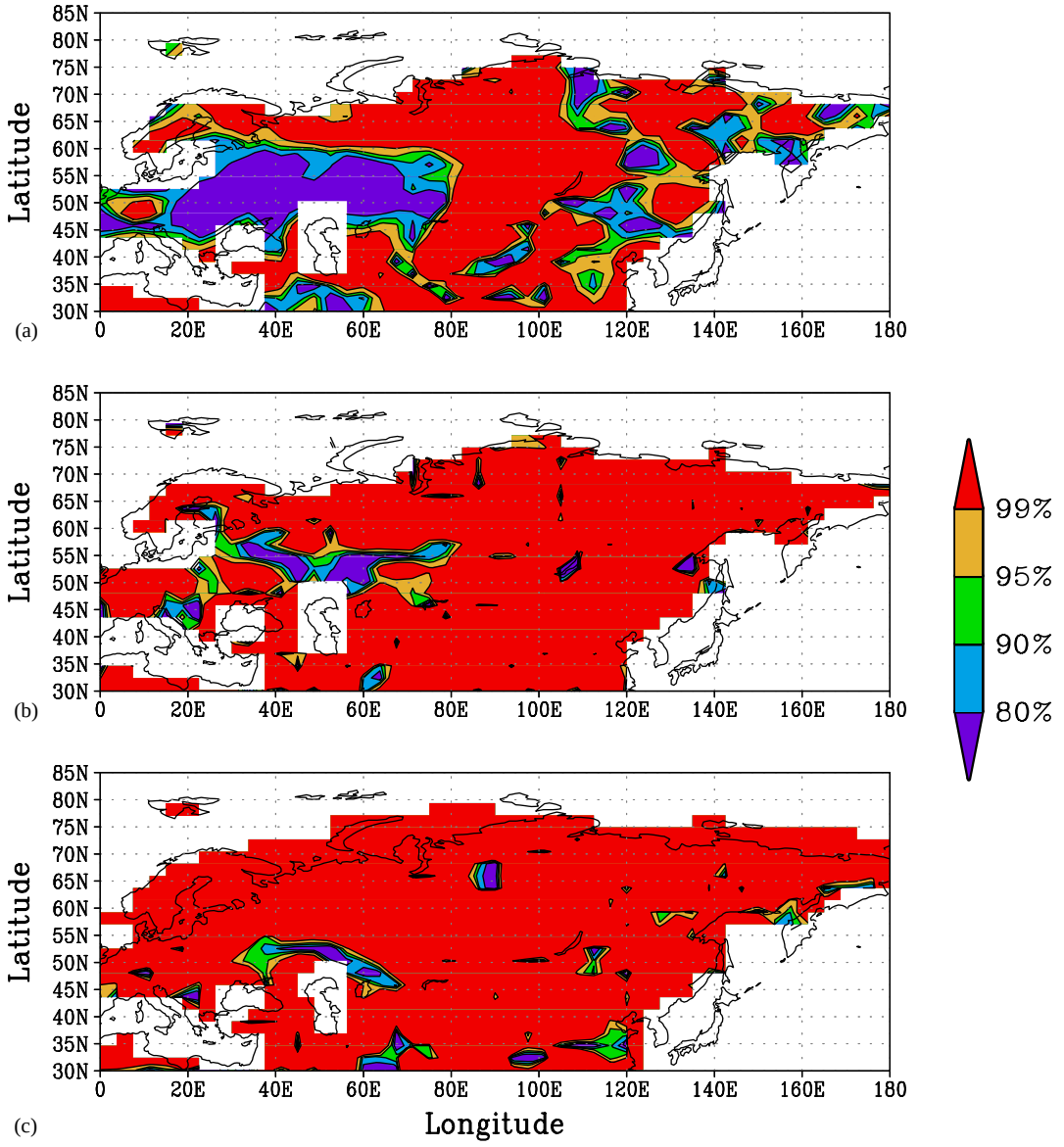

Fig. 5. Results of the Student *t*-test for statistical significance of the changes in simulated soil moisture for (a) 6000 BP, (b) 9000 BP, and (c) the LGM. Significance levels are shaded as indicated in the figure.

4. Discussion

4.1. Holocene climate

Simulated climate change across central Asia has a latitudinal dependence in the early and middle Holocene, a result also seen in the mid-Holocene, atmosphere-only simulations of PMIP (Masson et al., 1999). Higher obliquity and a summertime perihelion at the two simulated times of the Holocene have different effects on the seasonality of the Asian continent at different latitudes. In lower latitudes (up to approximately 50°N), strengthening of the summer monsoon winds and precipitation dominate the changes in moisture flux into southeastern Asia. Increased annual mean soil moisture in this region is consistent with the fact that desert margins bordering the Chinese Loess Plateau retreated northwestward of its present location (Fig. 8; see also Sun et al., 1998; Rokosh et al., 2003).

Farther west in the vicinity of the Black and Caspian Seas, wetter conditions are simulated and have been inferred for the mid-Holocene from reconstructions of the temperate deciduous forest biome (Tarasov et al., 1998). Based on this, a warmer and wetter summertime climate dominated during the early and middle Holocene.

North of 50°N, however, wintertime drying dominated the changes in soil moisture across west-central

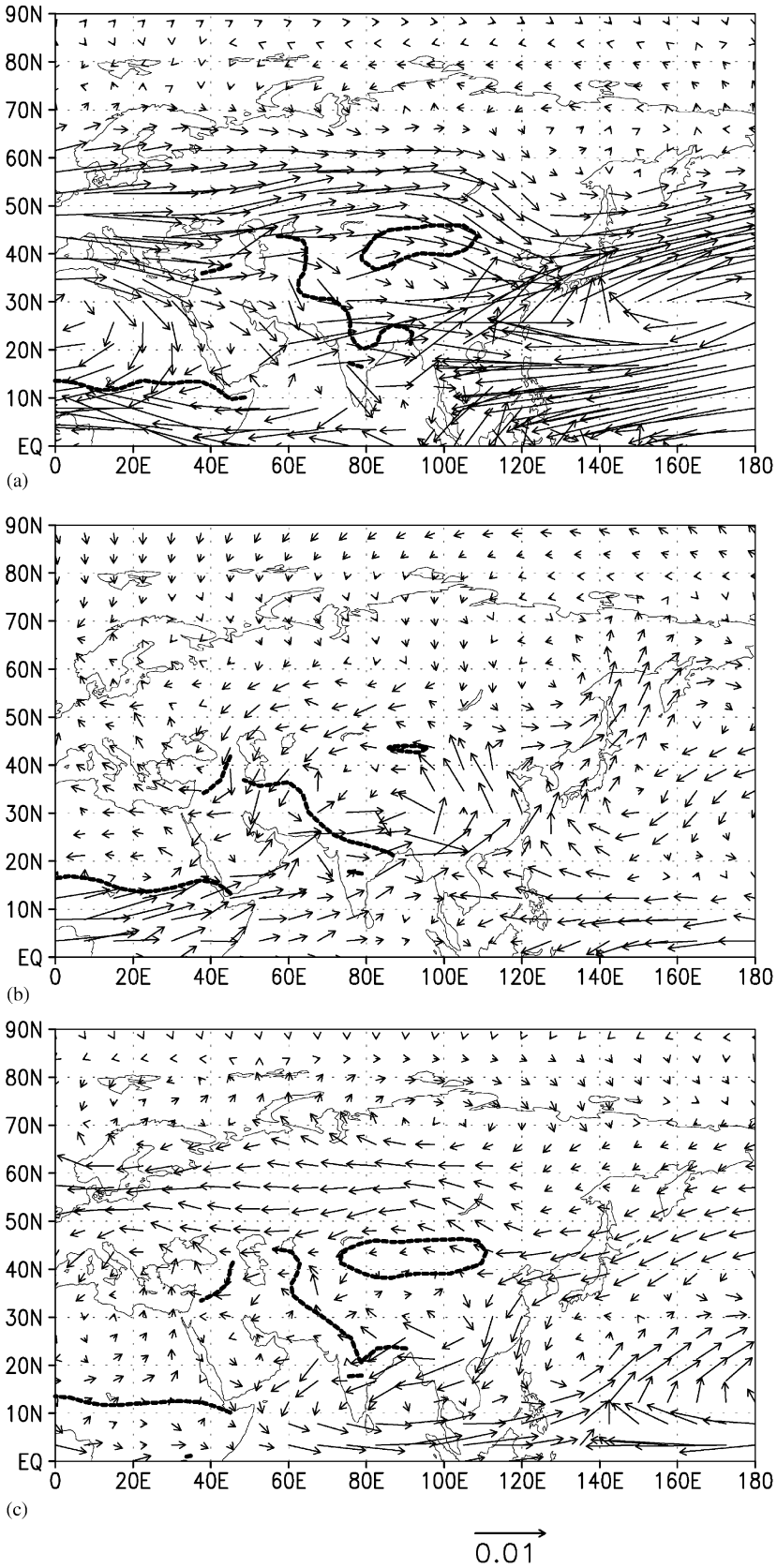

Fig. 6. Simulated moisture flux for today, defined as the tropospheric mean winds times the specific humidity. Units are g/g m/s and the vectors in all panels are scaled as indicated below the bottom panel. The 2-cm soil moisture curve (i.e., the desert margin proxy) is indicated in all three panels. (b) Difference in moisture transport in the early Holocene simulation (9000 BP minus control). (c) Difference in moisture transport in the LGM simulation (LGM minus control).

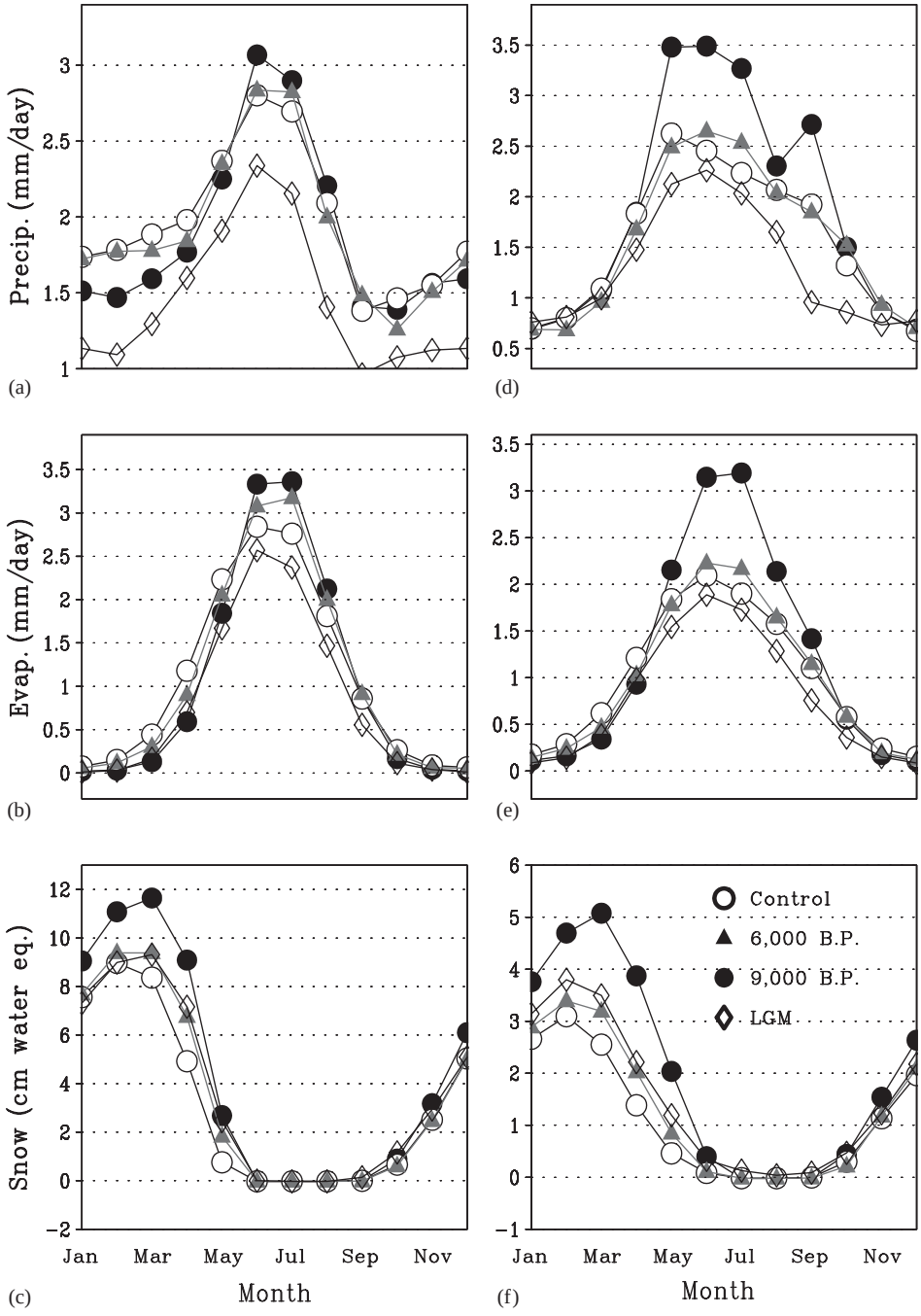

Fig. 7. (a) Simulated precipitation values (mm/day) over northern Asia (60–120°E, 45–65°N) in all four simulations (symbols for the simulations are shown in the bottom panel). (b) Evaporation (mm/day). (c) Snow cover (cm water equivalent). Equivalent values over southern Asia (60–120°E, 35–45°N) are given in panels (d)–(f).

Asia in both the early and mid-Holocene simulations. In these latitudes, there is evidence for drier conditions and colder winters from lake level data near the Baltic Sea (Harrison et al., 1996) and from central Kazakhstan (~52°N, 70°E; Tarasov et al., 1994; Harrison et al., 1996). Despite the fact that the boreal winter atmosphere is more baroclinic and, therefore, produces more transient mid-latitude eddies (Bush, 2003), precipitation during these events is primarily snowfall, not rain, because of colder wintertime temperatures. Hence, temperature modulation of that type of precipitation during midlatitude storms is an important factor in determining annual mean soil moisture in the model. Therefore, in these higher latitudes, colder and drier wintertime conditions dominated.

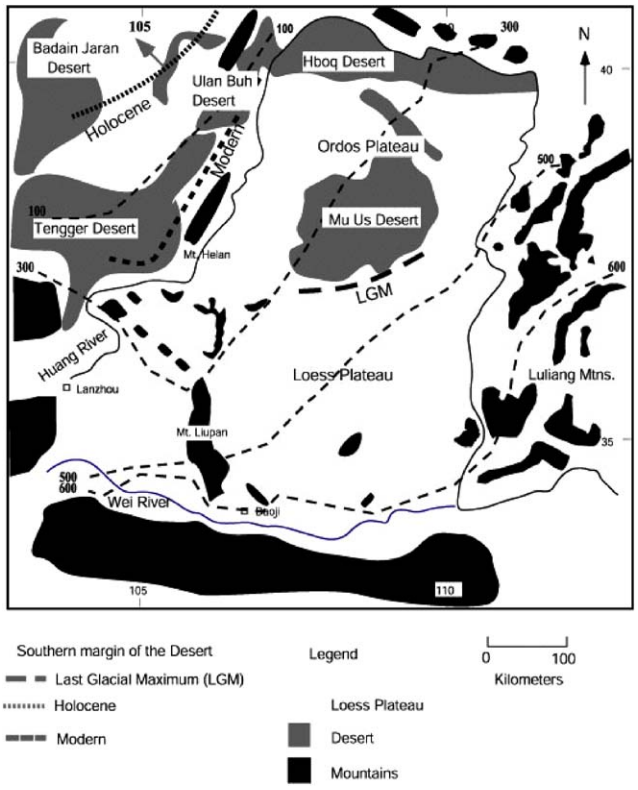

Fig. 8. Estimated locations of the southern limit of the desert margins near the Chinese Loess Plateau during the LGM, the Holocene Optimum and today. The arrow for the Holocene Optimum indicates the direction in which the margin is believed to be located (to date it has not yet been found). Data have been updated from those shown in Bush et al. (2002). Precipitation isohyets are after Zhao (1986). The MuUs and Hboq are not modern deserts; rather they were deserts during the last glacial period (Sun et al., 1999). Areas in white between the deserts indicate bedrock at the surface. The map is modified after USA Defense Mapping Agency Aerospace Center, 1987, Operational Navigation Chart Series ONC, Sheets F-7, F-8, G-8 and G-9, Edition 4, 1987.

In the Asian interior, summertime temperatures were warmer and wintertime temperatures were colder in the Holocene based on simulations (Fig. 9). The absence of mid-Holocene conifers from Kazakhstan in the Asian interior has been interpreted as a result of drying of the continental interior through either warmer summers or colder winters (Tarasov et al., 1997). The model simulations suggest that both of these conditions were satisfied in this region. Mid-Holocene climate reconstructions from the northern Russian Plain (Cheddadi et al., 1997) suggest that wintertime temperatures were warmer and this argues for warmer December–January–February temperatures over Scandinavia, along the coast of Northern Asia, and over eastern Yakutia (~65°N; ~140°E; Fig. 9c). However, warmer wintertime temperatures are not simulated over central and southern Yakutia, as has been inferred from pollen data (see Tarasov et al., 1998).

In the 9000 BP simulation, increased summertime warmth is simulated across Europe, west Siberia, and along the east coast of Asia (Fig. 10b). Nevertheless, colder temperatures are simulated across the Tibetan Plateau, even in the summertime. Simulated colder mean temperatures over the Tibetan and Mongolian Plateaus in the early Holocene would be conducive to glacier buildup and expansion. Primarily as a result of insolation changes, this cooling appears to be consistent with (or conducive to) the widespread cold event at ~8200 BP identified in the geological record (e.g., Alley et al., 1997).

In northwest Mongolia (48°40′N, 88°18′E), pollen and diatom records indicate that vegetation in the early Holocene (~9000 radiocarbon years or ~10,200 calendar years BP) was characterized by boreal conifer forest-steppe conditions. This was replaced in the mid-Holocene (~4000 radiocarbon years or ~4500 calendar years BP) by steppe conditions with a sharp reduction of forest (Tarasov et al., 2000a). Inspection of the simulated climate zones (Fig. 11) indicates that this region was characterized by a type D climate in the early Holocene simulation (temperate with year-round rainfall) whereas expansion of type B climate (semi-arid, steppe) occurs in the mid-Holocene simulation. Increased moisture in this region during the early Holocene is a consequence of the stronger summer Asian monsoon, which penetrates significantly farther into northwestern China and Mongolia (cf. Fig. 6b) as first suggested by Tarasov et al. (2000a) and supported by data from western Mongolia (Lehmkuhl and Haselein, 2000; Grunert et al., 2000). In fact, penetration of the simulated monsoon is so extensive in this region that wetter conditions reach the southeastern Altay Mountains, where lake level data indicate expanded paleoshorelines in the early Holocne but reduced lake levels by mid-Holocene time (Komatsu et al., 2001). These results agree well with the previous modeling work that showed a decreasing trend of positive precipitation anomalies over northwestern China from the early to mid-Holocene (An et al., 2000).

A variety of data from northern China on the southeastern Mongolian Plateau indicate that climate conditions went from cold and humid in the early Holocene to warm and humid in the mid-Holocene (Yu et al., 1998; Liu et al., 2001, 2002; Wang et al., 2001) resulting in northward and westward migration of the forest biomes (Yu et al., 2000). The model simulations indicate colder (cf. Fig. 11a) and wetter (cf. Fig. 4c) conditions than today for the early Holocene. For the mid-Holocene, wetter conditions than today prevailed (cf. Fig. 4b) but annual mean temperature was similar to today (cf. Fig. 9a). Climates in the simulated time periods also agree with the timing of humid phases during the so-called Holocene Megathermal (Chen et al.,

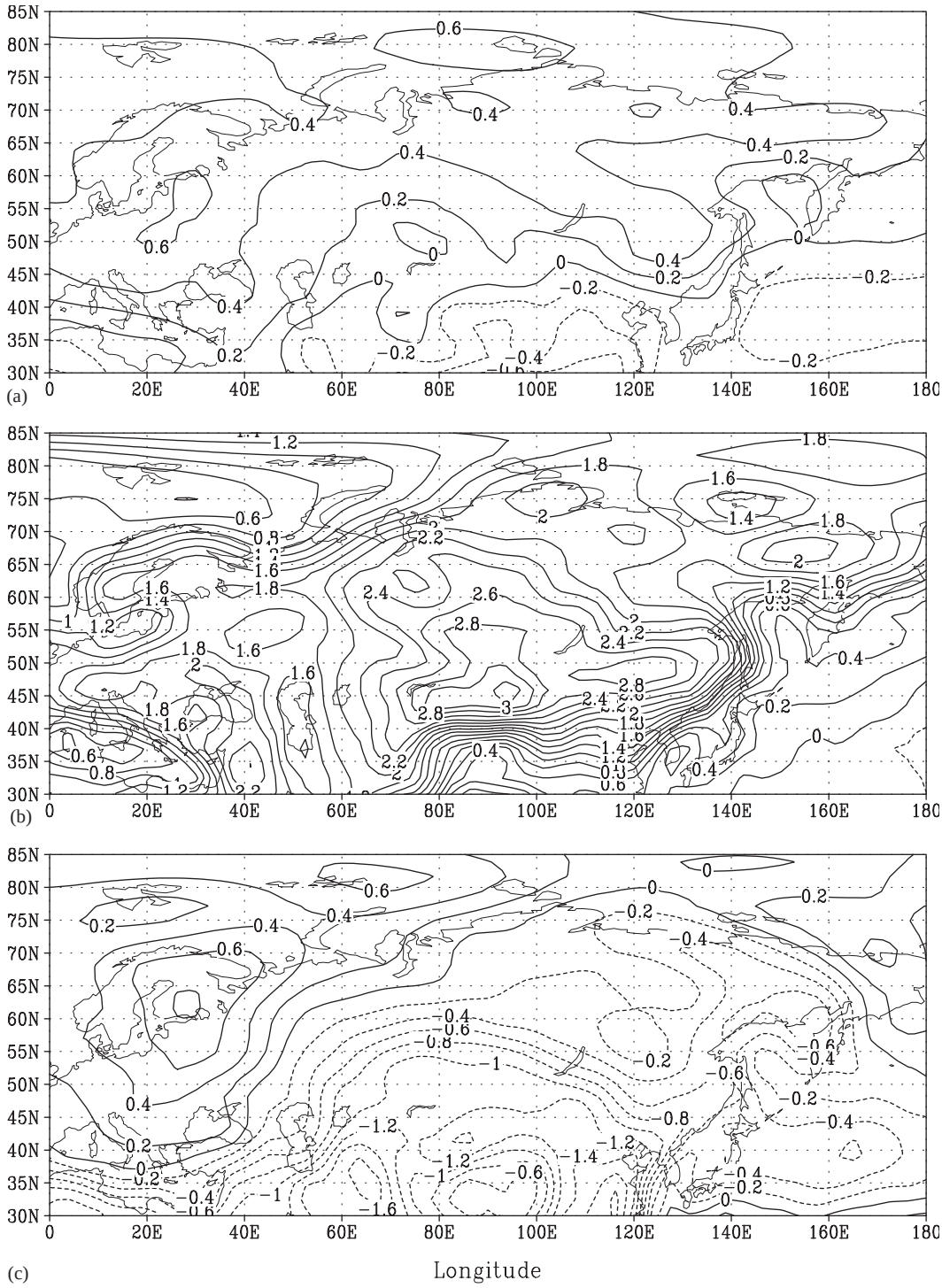

Fig. 9. (a) Simulated annual mean temperature anomaly (experiment minus today) for the mid-Holocene simulation. (b) June–July–August mean mid-Holocene temperature anomaly. (c) December–January–February mean mid-Holocene temperature anomaly. Units are °C with a contour interval of 0.2°C in all panels.

2003); the simulations do not, however, give any direct insight into what factors may have led to the arid phases (Peck et al., 2002; Chen et al., 2003), aside from the observation that in the mid-Holocene the boundary separating wetter southeast Asia from drier north-central Asia is in northwestern China (cf. Fig. 4). Since this margin shifts southeastward from 9000 BP to 6000 BP it is possible that, during the mid-Holocene, temporal fluctuations of this margin, related to insolation changes, may have been responsible (as might be inferred from the modeling results of An et al. (2000)).

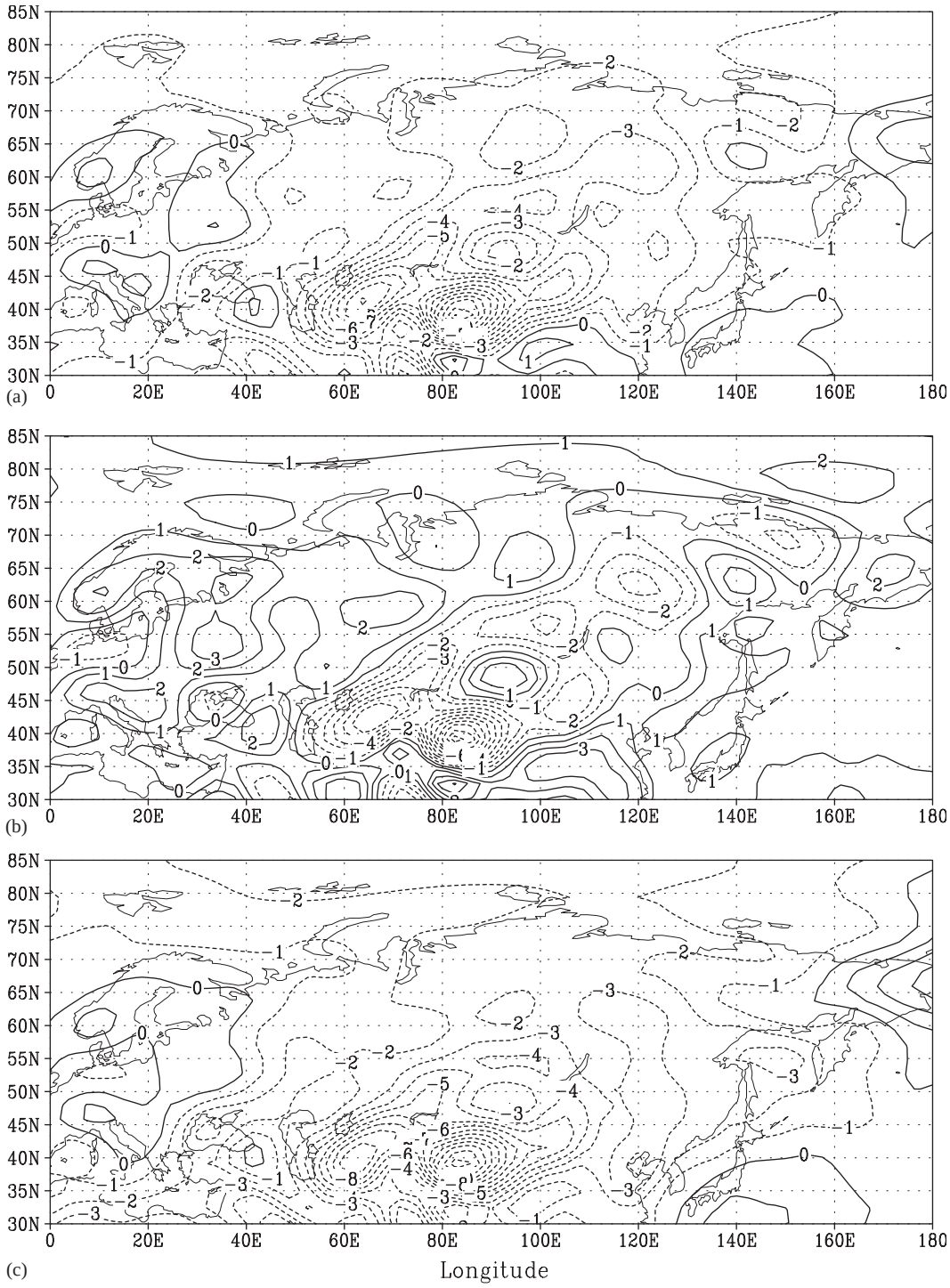

Fig. 10. (a) Simulated annual mean temperature anomaly (experiment minus today) for the early Holocene simulation. (b) June–July–August mean early-Holocene temperature anomaly. (c) December–January–February mean early-Holocene temperature anomaly. Units are °C with a contour interval of 1°C in all panels.

4.2. Last Glacial Maximum

Seasonal radiative forcing in the LGM simulation is comparable to that of today. Because of the reduced amount of atmospheric carbon dioxide and, consequently, colder temperatures and reduced specific humidities, there is a global decrease in precipitation (and evaporation), colder temperatures and reduced specific humidities. Exceptions to this reduced hydrological cycle occur where tropical land masses were

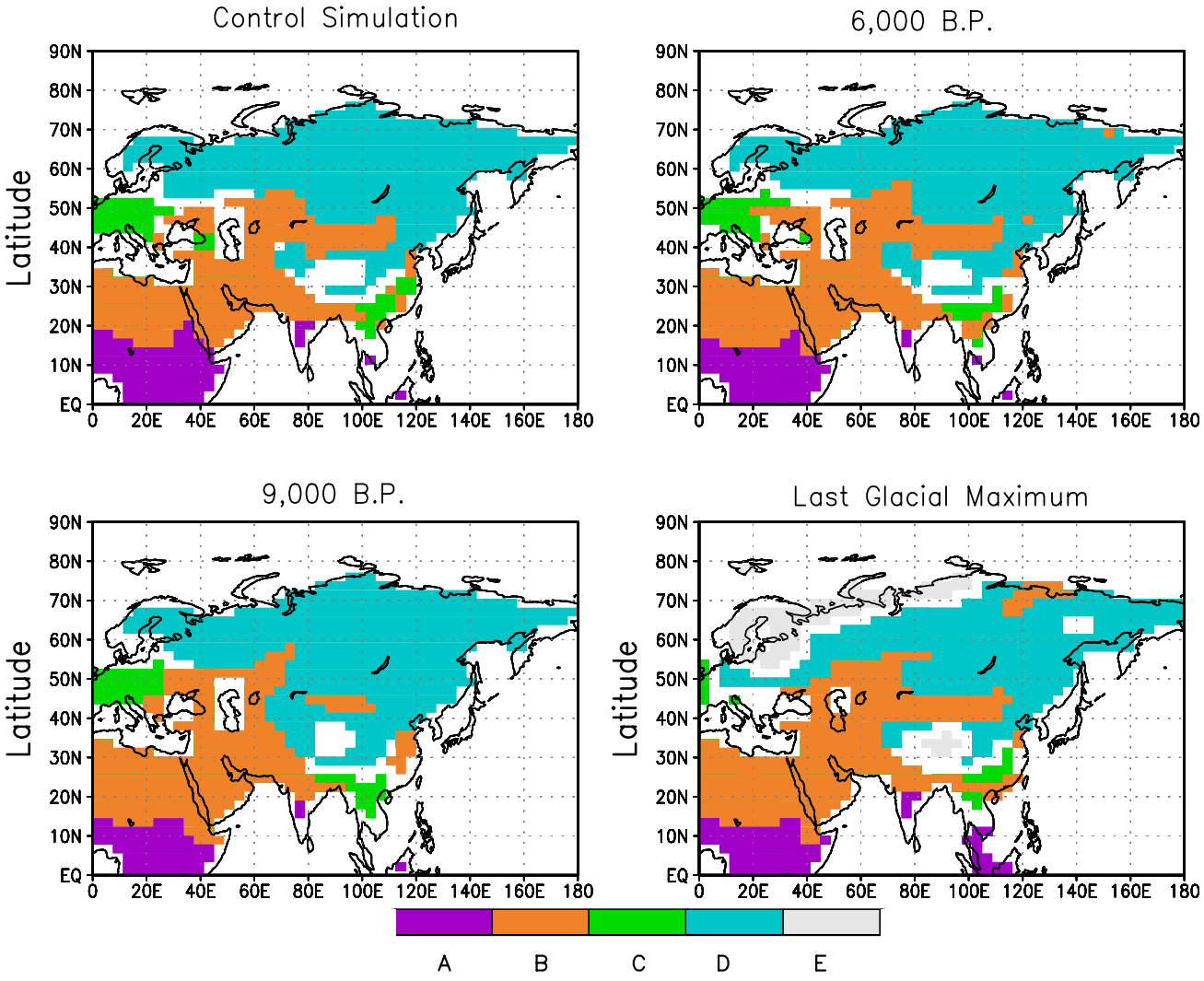

Fig. 11. Simulated Köppen climate zones for all simulations. A: Tropical; B: Dry; C: Temperate; D: Cold; and E: Polar. White areas are either Highland zones or regions where the numerical scheme failed to categorize the climate.

exposed, such as the Sunda Shelf and the South China Sea, where net freshwater flux was significantly increased (Bush and Fairbanks, 2003; see also Fig. 4 in Bush and Philander (1999)). The seasonal variability of precipitation, however, was comparable to today (cf. Fig. 7a). In addition, the westerly transport of water vapor into the Asian interior was significantly reduced because of the orographic blocking of the trade winds by the Fennoscandian ice sheet (cf. Fig. 6c).

Simulated seasonal temperatures at the LGM (Fig. 12) indicate that both summer and winter temperatures were significantly colder than today and would therefore be conducive to the observed southward expansion of tundra (Tarasov et al., 2000b). Similar results (~2–3° of annual mean cooling) were inferred for the region surrounding the Indian Ocean from PMIP model-data intercomparisons (Farrera et al., 1999). Over north-central Mongolia, colder mean temperatures and reduced soil moisture suggest that conditions were not favourable for the existence of forest (discussed in Tarasov et al., 2000b) and that permafrost could exist (Owen et al., 1998).

Evidence for large-scale drying in the Asian interior, particularly over the Siberian Plain, comes from biome reconstructions from pollen and plant macrofossil data (Tarasov et al., 2000b). Replacement of modern taiga by steppe across much of northern Eurasia at the LGM is consistent with simulated cooling and drying of the Asian interior and the northeastward expansion of the semi-arid/steppe B climate zone (cf. Fig. 11d). Southeastward expansion of the Gobi desert margin is consistent with the changes in Asian monsoon dynamics that have been analyzed previously (Bush, 2002), as well as with data indicating poor vegetation conditions over Northern Mongolia (Feng, 2001).

Wetter soil conditions are simulated for most of Europe at the LGM, despite a decrease in annual mean precipitation. This result appears to be common in numerical simulations (see the discussion in, e.g., Kageyama et al., 2001) although the dominance of steppe in this region at the LGM (Tarasov, 1999) suggests that seasonality of precipitation is a crucial factor (Prentice et al., 1992). Despite the simulated increase in soil moisture, there is a reduction of the subtropical C climate zone over much of Europe because of decreased summer temperatures (cf. Fig. 11d).

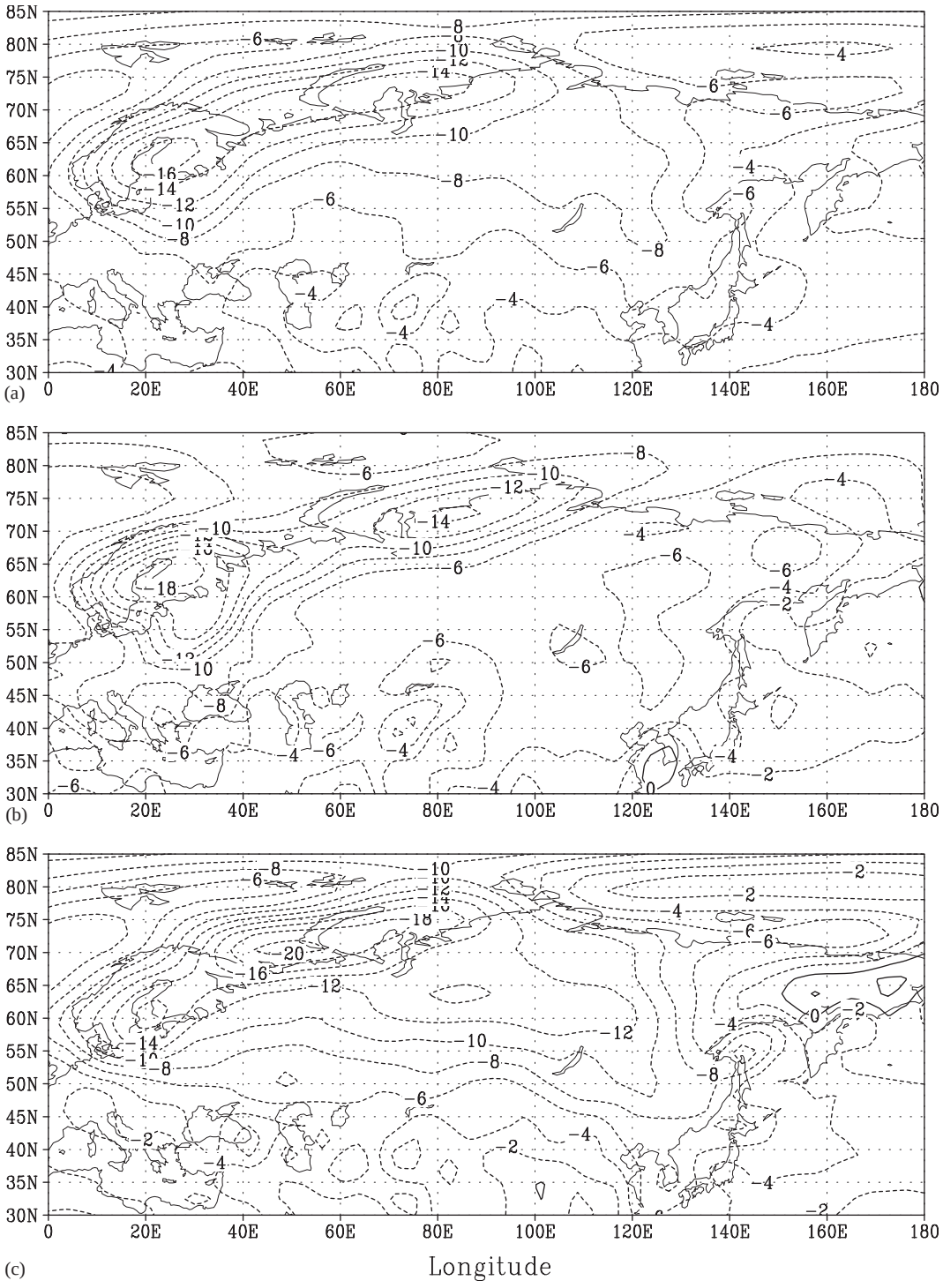

Fig. 12. (a) Simulated annual mean temperature anomaly (experiment minus today) for the LGM simulation. (b) June–July–August mean LGM temperature anomaly. (c) December–January–February mean LGM temperature anomaly. Units are °C with a contour interval of 2°C in all panels.

5. Summary and conclusions

In general, simulated changes in early and middle Holocene climate exhibit a pattern of spatial variability that was determined by a combination of radiative forcing and atmospheric circulation, as proposed by Xiao et al. (2002). Climates at higher latitudes were dominantly controlled by radiative forcing, and colder winters tend to dry central Asia despite increased summertime precipitation. The lower latitudes were, in general, wetter through a combination of increased seasonality (over far western Asia/Europe) and enhanced monsoon dynamics (over east Asia).

At the LGM, extensive drying of central and southeastern Asia was simulated. Diversion of the trade winds by the Fennoscandian ice sheet significantly reduced moisture transport into the Asian interior and, in combination with colder summer temperatures, produced more semi-arid/steppe conditions in the west Siberian Plain. Nevertheless, wetter soil conditions are simulated south of the ice sheet over Europe, despite the fact that the colder climate reduced the extent of the subtropical climate zone.

The fact that terrestrial records (e.g., loess–paleosol sequences, data from pollen and plant macrofossils) exhibit a degree of spatial variability through the Late Quaternary should not therefore be surprising. Within Asia, changes in regional climate led to the formation of loess in one location while paleosols developed in other locations.

The dynamic factors, described herein, that underpin the spatial variability of wetting/drying in the LGM and Holocene simulations may account, in part, for the variability in loess/paleosol deposition seen in the terrestrial records. To better understand the temporal and spatial variability over Asia, however, it would be necessary to either integrate a series of more closely spaced simulations or to perform one long simulation spanning the entire post-LGM interval. While this is at present impractical, it would nevertheless be the next step towards more clearly deciphering the complex terrestrial records.

Acknowledgements

A.B.G.B. acknowledges funding from NSERC G121210769 and the Climate System History and Dynamics Research Network Grant.

References

Alley, R.B., Mayewski, P.A., Sowers, T., Stuiver, M., Taylor, K.C., Clark, P.U., 1997. Holocene climatic instability: a prominent, widespread event 8200 yr ago. Geology 25, 483–486.

An, Z., Porter, S.C., Kutzbach, J.E., Xihao, W., Suming, W., Xiaodong, L., Xiaoqiang, L., Weijian, Z., 2000. Asynchronous Holocene optimum of the East Asian monsoon. Quaternary Science Reviews 19, 743–762.

Berger, A., Loutre, M.F., 1991. Insolation values for the climate of the last 10 million years. Quaternary Sciences Review 10 (4), 291–317.

Broccoli, A.J., Manabe, S., 1992. The effects of orography on midlatitude northern-hemisphere dry climates. Journal of Climate 5, 1181–1201.

Bush, A.B.G., 2002. A comparison of simulated monsoon circulations and snow accumulation in Asia during the mid-Holocene and at the Last Glacial Maximum. Global and Planetary Change 32, 331–347.

Bush, A.B.G., 2003. Baroclinic waves in Climates of the Earth's past. In: Velasco-Fuentes, O.U., Sheinbaum, J., Ochoa de la Torre, J.L. (Eds.), Nonlinear Processes in Geophysical Fluid Dynamics, Kluwer Academic Publishers, Dordrecht, The Netherlands, in press.

Bush, A.B.G., Fairbanks, R.G., 2003. Exposing the Sunda Shelf: tropical responses to eustatic sea level change. Journal of Geophysical Research–Atmospheres, in press.

Bush, A.B.G., Philander, S.G.H., 1999. The climate of the Last Glacial Maximum: results from a coupled atmosphere–ocean general circulation model. Journal of Geophysical Research 104, 24,509–24,525.

Bush, A.B.G., Rokosh, D., Rutter, N., Moodie, T.B., 2002. Desert margins near the Chinese Loess Plateau during the mid-Holocene and at the Last Glacial Maximum: a model-data intercomparison. Global and Planetary Change 32, 361–374.

Cheddadi, R., Yu, G., Guiot, J., Harrison, S.P., Prentice, I.C., 1997. The climate of Europe 6000 years ago. Climate Dynamics 13, 1–9.

Chen, C.-T.A., Lan, H.-C., Lou, J.-Y., Chen, Y.-C., 2003. The dry Holocene megathermal in Inner Mongolia. Palaeogeography, Palaeoclimatology, Palaeoecology 193, 181–200.

Climate: Long-Range Investigation, Mapping, and Prediction (CLIMAP) Project Members, 1981. Seasonal reconstructions of the Earth's surface at the Last Glacial Maximum. Map and Chart Series MC-36. Geological Society of America, Boulder, CO.

Crowley, T.J., 1984. Atmospheric circulation patterns during glacial inception: a possible candidate. Quaternary Research 21, 105–110.

Fairbanks, R.G., 1989. A 17,000 year glacio-eustatic sea level record: influence of glacial melting rates on Younger Dryas event and deep-ocean circulation. Nature 342, 637–642.

Fanning, A.F., Weaver, A.J., 1996. An atmospheric energy-moisture balance model: climatology, interpentadal climate change, and coupling to an ocean general circulation model. Journal of Geophysical Research 101, 15,111–15,128.

Farrera, I., Harrison, S.P., Prentice, I.C., Ramstein, G., Juiot, J., Bartlein, P.J., Bonnefille, R., Bush, M., Cramer, W., von Grafenstein, U., Holmgren, K., Hooghiemstra, H., Hope, G., Jolly, D., Lauritzen, S.-E., Ono, Y., Pinot, S., Stute, M., Yu, G., 1999. Tropical climates at the Last Glacial Maximum: a new synthesis of terrestrial palaeoclimate data. I. Vegetation, lake-levels and geochemistry, 823–856.

Feng, Z.-D., 2001. Gobi dynamics in the Northern Mongolian Plateau during the past 20,000+ yr: preliminary results. Quaternary International 76/77, 77–83.

Gordon, C.T., Stern, W., 1982. A description of the GFDL global spectral model. Monthly Weather Review 110, 625–644.

Grunert, J., Lehmkuhl, F., Walther, M., 2000. Paleoclimatic evolution of the Uvs Nuur basin and adjacent areas (Western Mongolia). Quaternary International 65/66, 171–192.

Guo, Z.T., Liu, T.S., Fedoroff, N., Wei, L.Y., Ding, Z.L., Wu, N.Q., Lu, H.Y., Jian, W.Y., An, Z.S., 1998. Climate extremes in loess of China coupled with the strength of deep-water formation in the North Atlantic. Global and Planetary Change 18, 113–128.

Hahn, D.G., Manabe, S., 1975. The role of mountains in the south Asian monsoon circulation. Journal of the Atmospheric Sciences 32, 1515–1541.

Hall, N.M.J., Valdes, P.J., Dong, B., 1996. The maintenance of the last great ice sheets: a UGAMP GCM study. Journal of Climate 9, 1004–1019.

Harrison, S.P., Yu, G., Tarasov, P.E., 1996. Late Quaternary lake-level records from northern Eurasia. Quaternary Research 45, 138–159.

Holton, J.R., 1979. An Introduction to Dynamic Meteorology, 2nd Edition. International Geophysics Series, Vol. 23. Academic Press, Inc., New York, 391pp.

Hoskins, B.J., Rodwell, M.J., 1995. A model of the Asian summer monsoon. Part I: the global scale. Journal of the Atmospheric Sciences 52, 1329–1340.

Kageyama, M., Peyron, O., Pinot, S., Tarasov, P., Guiot, J., Joussaume, S., Ramstein, G., 2001. The Last Glacial Maximum climate over Europe and western Siberia: a PMIP comparison between models and data. Climate Dynamics 17, 23–43.

Kohfeld, K.E., Harrison, S.P., 2000. How well can we simulate past climates? Evaluating the models using global palaeoenvironmental datasets. Quaternary Science Reviews 19, 321–346.

Komatsu, G., Brantingham, P.J., Olsen, J.W., Baker, V.R., 2001. Paleoshoreline geomorphology of Boon Tsagaan Nuur, Tsagaan Nuur and Orog Nuur: the Vallay of Lakes, Mongolia. Geomorphology 39, 83–98.

Kutzbach, J.E., Guetter, P.J., Ruddiman, W.F., Prell, W.L., 1989. Sensitivity of climate to Late Cenozoic uplift in Southern Asia and the American West—numerical experiments. Journal of Geophysical Research–Atmospheres 94 (D15), 18,393–18,407.

Lehmkuhl, F., Haselein, F., 2000. Quaternary paleoenvironmental change on the Tibetan Plateau and adjacent areas (Western China and Western Mongolia). Quaternary International 65/66, 121–145.

Levitus, S., 1982. Climatological atlas of the world ocean. NOAA Prof. Paper 13. US Govt. Print. Office, Washington, DC, 173pp.

Limpasuvan, V., Hartmann, D.L., 2000. Wave-maintained annular modes of climate variability. Journal of Climate 13, 4414–4429.

Liu, H., Cui, H., Huang, Y., 2001. Detecting Holocene movements of the woodland-steppe ecotone in northern China using discriminant analysis. Journal of Quaternary Science 16 (3), 237–244.

Liu, H., Xu, L., Cui, H., 2002. Holocene history of desertification along the woodland-steppe border in Northern China. Quaternary Research 57, 259–270.

Lu, H.Y., VanHuissteden, K.O., An, Z.S., Nugteren, G., Vandenberghe, J., 1999. East Asia winter monsoon variations on a millennial time-scale before the last glacial-interglacial cycle. Journal of Quaternary Science 14, 101–110.

Lu, H.Y., VanHuissteden, K.O., Zhou, J., Vandenberghe, J., Liu, X.D., An, Z.S., 2000. Variability of East Asian winter monsoon in Quaternary climatic extremes in North China. Quaternary Research 54, 321–327.

Lu, H.Y., Sun, D.H., 2000. Pathways of dust input to the Chinese Loess Plateau during the last glacial and interglacial periods. Catena 40, 251–261.

Maher, B.A., MengYu, H., Roberts, H.M., Wintle, A.G., 2003. Holocene loess accumulation and soil development at the western edge of the Chinese Loess Plateau: implications for magnetic proxies of palaeorainfall. Quaternary Science Reviews 22, 445–451.

Masson, V., Cheddadi, R., Braconnot, P., Joussaume, S., Texier, D., 1999. PMIP participants, Mid-Holocene climate in Europe: what can we infer from PMIP model-data comparisons?

Meehl, G.A., Gent, P.R., Arblaster, J.M., Otto-Bleisner, B.L., Brady, E.C., Craig, A., 2001. Factors that affect the amplitude of El Niño in global coupled climate models. Climate Dynamics 17, 515–526.

Munk, W., Wunsch, C., 1998. Abyssal recipes II: energetics of tidal and wind mixing. Deep-Sea Research I 45, 1977–2010.

Owen, L.A., Richards, B., Rhodes, E.J., Cunningham, W.D., Windley, B.F., Badamgarav, J., Dorjnamjaa, D., 1998. Relic permafrost structures in the Gobi of Mongolia: age and significance. Journal of Quaternary Science 13 (6), 539–547.

Pacanowsi, R.C., Philander, S.G.H., 1981. Parameterization of vertical mixing in numerical models of tropical oceans. Journal of Physical Oceanography 11, 1443–1451.

Pacanowski, R.C., Dixon, K., Rosati, A., 1991. The GFDL Modular Ocean Model user guide, GFDL Ocean Group Technical Report 2, Geophys. Fluid Dyn. Lab, Princeton, NJ.

Peck, J.A., Khosbayar, P., Fowell, S.J., Pearce, R.B., Ariunbileg, S., Hansen, B.C.S., Soninkhishig, N., 2002. Mid to Late Holocene climate change in north central Mongolia as recorded in the sediments of Lake Telmen. Palaeogeography, Palaeoclimatology, Palaeoecology 183, 135–153.

Peltier, W.R., 1994. Ice age paleotopography. Science 265, 195–201.

Porter, S.C., An, Z.S., 1995. Correlation between climate events in the North Atlantic and China during last glaciation. Nature 375, 305–308.

Prentice, I.C., Guiot, J., Harrison, S.P., 1992. Mediterranean vegetation, lake levels and palaeoclimate at the Last Glacial Maximum. Nature 360, 658–660.

Press, W.H., Teukolsky, S.A., Vetterling, W.T., Flannery, B.P., 1992. Numerical Recipes. The Art of Scientific Computing. 2nd Edition. Cambridge University Press, Cambridge, 963pp.

Rack, F.R., Rutter, N.W., Bush, A.B.G., Rokosh, D., Ding, Z., 2000. Linking palaeoclimate ocean and continental (loess) records. Canadian Journal of Earth Sciences 37 (5), 831–848.

Rodwell, M.J., Hoskins, B.J., 1995. A model of the Asian summer monsoon. Part II: Cross-equatorial flow and PV behavior. Journal of the Atmospheric Sciences 52, 1341–1356.

Rokosh, D., Bush, A.B.G., Rutter, N.W., Ding, Z., Sun, J., 2003. Hydrologic and geologic factors that influenced spatial variations in loess deposition in China during the last interglacial–glacial cycle: results from proxy climate and GCM analysis. Palaeogeography, Palaeoclimatology, Palaeoecology 193, 249–260.

Rutter, N.W., 1992. Presidential Address, XIII INQUA Congress 1991: Chinese loess and global change. Quaternary Science Reviews 11, 275–281.

Rutter, N.W., Rokosh, D., Evans, M.E., Little, E.C., Chlachula, J., Velichko, A., 2003. Correlation and interpretation of paleosols and loess across European Russia and Asia over the last interglacial–glacial cycle. Quaternary International, in press.

Sun, J.M., Ding, Z.L., Liu, T.S., 1995. The environmental evolution of the desert-loess transitional zone over the last glacial–interglacial cycle. In Scientia Geologica Sinica, Science Press, Beijing, China pp. 1–8.

Sun, J.M., Ding, Z.L., Liu, T.S., 1998. Desert distribution during the glacial maximum and climatic optimum: example of China. Episodes 21, 28–30.

Sun, J.M., Ding, Z.L., Liu, T.S., Rokosh, D., Rutter, N.W., 1999. 580,000-year environmental reconstruction from aeolian deposits at the Mu Us desert margin, China. Quaternary Science Reviews 18, 1351–1364.

Tarasov, P.E., Harrison, S.P., Saarse, L., Pushenko, M.Ya., Andreev, A.A., Aleshinskaya, Z.V., Davydova, N.N., Dorofeyuk, N.I., Efremov, Yu.V., Khomutova, V.I., Sevastyanov, D.V., Tamosaitis, J., Uspenskaya, O.N., Yakushdo, O.F., Tarasova, I.V., 1994. Lake status records from the Former Soviet Union and Mongolia: data base documentation. NOAA Paleoclimatol. Publ. Ser. Report 2, Boulder, CO, 274pp.

Tarasov, P.E., Jolly, D., Kaplan, J.O., 1997. A continuous Late Glacial and Holocene record of vegetation changes in Kazakhstan. Palaeogeography, Palaeoclimatology, Palaeoecology 136, 281–292.

Tarasov, P., Dorofeyuk, N., Metel'Tseva, E., 2000a. Holocene vegetation and climate changes in Hoton-Nur basin, northwest Mongolia. Boreas 29, 117–126.

Tarasov, P., Volkova, V.S., Webb III, T., Guiot, J., Andreev, A.A., Bezusko, L.G., Bezusko, T.V., Bykova, G.V., Dorofeyuk, N.I., Kvavadze, E.V., Osipova, I.M., Panova, N.K., Sevastyanov, D.V., 2000b. Last Glacial Maximum biomes reconstructed from pollen and plant macrofossil data from northern Eurasia. Journal of Biogeography 27, 609–620.

Tarasov, P., Webb III, T., Andreev, A.A., Afanas'eva, N.B., Berezina, N.A., Bezusko, L.G., Blyakharchuk, T.A., Bolikhovskaya, N.S., Cheddadi, R., Chernavskaya, M.M., Chernova, G.M., Dorofeyuk, N.I., Dirksen, V.G., Elina, G.A., Filimonova, L.V., Glebov, F.Z., Guiot, J., Gunova, V.S., Harrison, S.P., Jolly, D., Khomutova, V.I., Kvavadze, E.V., Osipova, I.M., Panova, N.K., Prentice, I.C., Saarse, L., Sevastyanov, D.V., Volkova, V.S., Zernitskaya, V.P., 1998. Present-day and mid-Holocene biomes reconstructed from pollen and plant macrofossil data from the former Soviet Union and Mongolia. Journal of Biogeography 25, 1029–1053.

Thompson, D.W.J., Wallace, J.M., 2000. Annular modes in the extratropical circulation. Part I: Month-to-month variability. Journal of Climate 13, 1000–1016.

Thompson, L.G., Mosley-Thompson, E., Davis, M.E., Lin, P.-N., Henderson, K.A., Cole-Dai, J., Bolzan, J.F., Liu, K.-b., 1995. Late Glacial Stage and Holocene tropical ice core records from Huascaran, Peru. Science 269, 46–50.

Toole, J.M., McDougall, T.J., 2001. Mixing and stirring in the ocean interior. In: Siedlor, G., Church, J., Gould, J. (Eds.), Ocean Circulation and Climate. Academic Press, San Diego, pp. 337–355.

USA Defense Mapping Agency Aerospace Center, 1987. Operational Navigation Chart, Sheets F-7, F-8, G-8, G-9. US Department of Defense.

Vandenberghe, J., An, Z.S., Nugteren, G., Lu, H.Y., VanHuissteden, K., 1997. New absolute time scale for the Quaternary climate in the Chinese loess region by grain-size analysis. Geology 25, 35–38.

Wang, H., Lui, H., Cui, H., Abrahamsen, N., 2001. Terminal Pleistocene/Holocene paleoenvironmental changes revealed by mineral-magnetism measurements of lake sediments for Dali Nor area, southeastern Inner Mongolia Plateau, China. Palaeoclimatology, Palaeoecology 170, 115–132.

Washington, W.M., Parkinson, C.L., 1986. An Introduction to Three-Dimensional Climate Modelling. University Science Books, California, 422pp.

Wright, H.E.Jr., Kutzbach, J.E., Webb III, T., Ruddiman, W.F., Street-Perrott, F.A., Bartlein, P.J. (Eds.), 1993. Global Climates since the Last Glacial Maximum, University of Minnesota Press, Minneapolis, 569pp.

Wunsch, C., 2000. Oceanography: Moon, tides and climate. Nature 405, 743–744.

Xiao, J., Nakamura, T., Lu, H., Zhang, G., 2002. Holocene climate changes over the desert/loess transition of north-central China. Earth and Planetary Science Letters 197, 11–18.

Yu, G., Prentice, I.C., Harrison, S.P., Sun, X., 1998. Pollen-based biome reconstructions for China at 0 and 6000 years. Journal of Biogeography 25, 1055–1069.

Yu, G., Chen, X., Ni, J., Cheddadi, R., Guiot, J., Hans, H., Harrison, S.P., Huang, C., Ke, M., Kong, Z., Li, S., Li, W., Liew, P., Liu, G., Liu, J., Liu, Q., Liu, K.-B., Prentice, I.C., Qui, W., Ren, G., Song, C., Sugita, S., Sun, X., Tang, L., Van Campo, E., Xia, Y., Xu, Q., Yan, S., Yang, X., Zhao, J., Zheng, Z., 2000. Palaeovegetation of China: a pollen data-based synthesis for the mid-Holocene and last glacial maximum. Journal of Biogeography 27, 635–664.

Zhao, S., 1986. Physical Geography of China. Science Press, Beijing. Wiley, New York, 209pp.